Review

Automated Detection of Schizophrenia using Deep Learning: A Review for the last decade

Manish Sharma[1], Ruchit Kumar Patel[1], Akshat Garg[1], Ru SanTan[2], and U Rajendra Acharya[3,4,5]

1 Department of Electrical and Computer Science Engineering, Institute of Infrastructure Technology Research and Management, Ahmedabad 380026, India; ruchitkumar.patel.19e@iitram.ac.in (Student); akshat.garg.19e@iitram.ac.in (Student)

2 Department of Cardiology, National Heart Centre Singapore, Singapore 169609, Singapore; tanrsnhc@gmail.com

3 Department of Electronics and Computer Engineering, Ngee Ann Polytechnic, Singapore 639798, Singapore; aru@np.edu.sg

4 Department of Bioinformatics and Medical Engineering, Asia University, Taichung 41354, Taiwan

5 Department of Biomedical Engineering, School of Science and Technology, Singapore 639798, Singapore

Correspondence: manishsharma.iitb@gmail.com

‡ These authors contributed equally to this work.

Received xxxxxx
Accepted for publication xxxxxx
Published xxxxxx

Abstract

Schizophrenia (SZ) is a devastating mental disorder that disrupts higher brain functions like thought, perception, etc., with a profound impact on the individual's life. Deep learning (DL) can detect SZ automatically by learning signal data characteristics hierarchically without the need for feature engineering associated with traditional machine learning. We performed a systematic review of DL models for SZ detection. Various deep models like long short-term memory, convolution neural networks, AlexNet, etc., and composite methods have been published based on electroencephalographic signals and structural and/or functional magnetic resonance imaging acquired from SZ patients and healthy patients control subjects in diverse public and private datasets. The studies, the study datasets, and model methodologies are reported in detail. In addition, the challenges of DL models for SZ diagnosis and future works are discussed.

Keywords: Schizophrenia, deep learning, electroencephalography, long short-term memory, convolutional neural networks, functional magnetic resonance imaging

1. Introduction

Schizophrenia (SZ) is a devastating mental disorder that disrupts higher brain functions like thought, memory, perception, speech, etc., profoundly impacting the individual's relationships, livelihood, and lifestyle [1]. SZ can present with positive, negative, or cognitive symptoms [2,3], which typically manifest between the ages of 16 and 30. Early recognition of these symptoms and initiation of treatment are important to minimize the long-term deleterious effects of SZ-induced behavioral changes [1]. Pharmaceutical treatment, based on neurochemical signaling involving acetylcholine, gamma aminobutyric acid, glutamate, and serotonin re-uptake and release, is the mainstay of SZ management [4]. Adjunctive nonpharmacological therapy assists patients in coping with their symptoms and achieving a socially acceptable psychosocial functioning level. The diagnosis of SZ requires a detailed psychiatric examination during which a trained psychiatrist interviews the patient to elicit specific behavioral symptoms such as impaired functioning, hallucinations, and disordered speech [1,5]. The accuracy is confounded

by the subjective nature of the symptoms, intra- and inter-observer biases, and the potential for SZ to co-exist with other psychiatric disorders, which increases the probability of diagnostic error [6]. Further, individuals, with a positive family history of SZ may present with a premorbid or prodromal phase before the development of frank psychosis [7]. In such cases, as well as in established SZ, evidence of altered brain activity and/or anatomy on electroencephalography (EEG) [8] and magnetic resonance imaging (MRI), respectively, may help corroborate clinical observations.

EEG measures electrical potentials arising from different regions of the brain using a spatial array of multiple electrodes placed on the scalp, which typically number 10 to 20 and are labelled with letters that represent the underlying brain lobes: "C", central; "T", temporal; "F", frontal; "O", occipital; and "P", parietal [9-12]. The raw EEG signals are input to an analog-to-digital converter and amplifier before being pre-processed to filter the data and remove artifacts [9]. Experts categorize the readout based on frequency, amplitude, shape, and scalp position [9]. Characteristic patterns of EEG waveforms at rest or after provocation, i.e., event-related potentials (ERPs), may be associated with conditions like epilepsy, Alzheimer's disease, attention deficit disorder, and SZ [4]. The standardized collection of EEG signals constitutes a comprehensive data structure [4] that is eminently amenable for clinical interpretation and artificial intelligence-enabled approaches for automated computer-aided diagnosis.

MRI yields granular information about the structure and function of the brain, and can be categorized into structural (sMRI), perfusion (pMRI), diffusion-weighted MRI (dMRI), as well as functional (fMRI). sMRI depicts brain grey and white matter with fine spatial resolution, allowing accurate quantification of anatomical pathology in regions of interest in diverse diseases. In SZ, there is the reduction of grey matter volume, particularly in the frontal and temporal regions of the brain [13]; as well as deeper white matter loss, which comprises nerve fibers and cells that play crucial roles in the central nervous system signal reception and transmission [13]. In pMRI, quantitative imaging of hemodynamic parameters like cerebral blood flow, mean transit time, and cerebral blood volume enables the noninvasive determination of regional cerebral perfusion [14,15], which is impaired in cerebrovascular and other brain diseases, including SZ [4]. Indeed, pMRI has been used to assess the efficacy of SZ-related pharmacological therapies through their effects on blood circulation [4]. dMRI uses diffusion tensor imaging to map water diffusion in the brain. The diffusion tensor is extremely sensitive to alterations at cellular and microstructural levels. It, among other things, determines the degree and extent of diffusion anisotropy and its orientation [4], which are used in white matter tractography to construct brain connectivity models. Analysis of the white matter fiber tract may detect characteristic patterns of disruptions in connectivity between brain regions in various disease states, including SZ [16,17]. Unlike sMRI, pMRI, and dMRI, which are commonly performed in the clinical setting, fMRI is largely research-based. Using blood oxygenation level-dependent imaging, fMRI can detect spatiotemporally resolved, cerebral blood oxygen concentration increases, which denote heightened activity in response to spontaneous or task-induced regulation of brain metabolism [4]. Technical advances have considerably enhanced the signal-to-noise ratio, allowing for detailed interrogation of regional brain activation at different cognitive states in health and disease [4], including in SZ [18].

MRI and EEG may uncover complementary evidence of structural or functional perturbations to support the diagnosis of SZ in some patients. Positron emission tomography, coupled with either computed tomography or MRI, can also track regional brain activity using radioactive metabolic or biochemical tracers [4], which are exquisitely sensitive to aberrant metabolism in the early stages of the disease e.g., cancer, brain disorders, etc. The use is, however, limited by the high cost and need for ionizing radiation. Data readout from EEG and MRI requires expert interpretation; their volume and density render the task onerous and manually intensive. As a result, machine (ML), including deep learning (DL), models are increasingly being employed for the automated detection of SZ, using MRI and EEG-derived signals with or without subjective assessments of patient stance, expression, verbiage, mindset, and behaviors [4]. Conventional ML models have been previously reviewed [8,4]. In traditional ML, an algorithm is first chosen and developed with data from the training set with specified features extracted and selected for classification [19-22]. The extraction and selection of features exert a significant impact on the performance of ML learning algorithms: biased feature extraction can lead to inaccurate class discrimination [23].

In contrast to traditional ML, DL does not require pre-determined feature engineering. Instead, the optimum traits are "learned" autonomously in relation to the job at hand: the learning and categorization are achieved in a single shot [24] versus several requisite steps such as pre-processing, feature selection, and extraction in traditional ML. Accordingly, the input data is robust to normal variations, which means that different data types or applications can share the same DL model, i.e., transfer learning [25]. Although a single-layer neural network may approximate the ground truth, adding extra hidden layers can potentially refine the model to optimize accuracy [26]. The main limitations of DL are high computational complexity [27] compared with traditional ML [28] and the requirement for a large volume of training data, which can be difficult to obtain. The latter can sometimes be surmounted by transfer learning, where DL models pre-trained on accessible large databases are used to classify unseen data [25], which is an effective strategy when training data are scarce. DL is thus scalable and can potentially automate the learning of selected features for many applications. Not surprisingly, DL has garnered increasing

popularity for diverse medical and healthcare applications, including mental health disorders [29-31] and neuroimaging [32]. In this work, we aim to perform a systematic review of contemporary DL techniques for detecting SZ using various biomedical signals that will serve as a resource for researchers in the field.

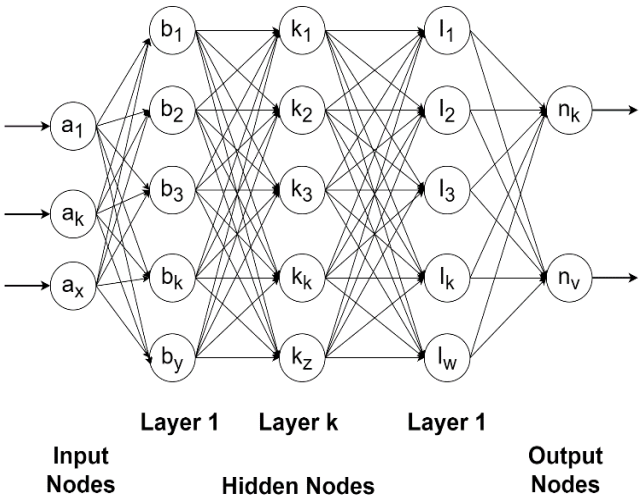

Figure 1. Deep learning model. It shows input layers represented with node "a", Layer 1 represented with node "b" and the layers following it are hidden layers until layer I. There are k hidden layers with nodes represented with subscript, i = 1,2,3….Z to it. Layer n is the output layer.

Our contributions are:

• To our knowledge, this is the first review focusing on DL techniques for detecting SZ.

• Summary of state-of-the-art DL methods, which will interest researchers in the field.

• Establish a frame of reference for evaluating fresh discoveries, and as a corollary, recommend appropriate DL approaches for specific applications that will serve as initial ideas for subsequent experiments.

• Critique the limitations of contemporary DL-based methods and suggestions for potential workarounds.

• Commentary on future prospects for leveraging complementary EEG and neuroimaging signals to diagnose SZ using artificial intelligence algorithms.

The rest of the article is structured as follows: Section 2 details the literature search methodology; Section 3, the results, including different databases used in the studies; Section 4, the various DL algorithms used for other input signals; Section 5, discussion; Section 6, the challenges in DL; Section 7, future works; and Section 8, conclusion.

2. Literature Search

We conducted a systematic review of the literature published on Google Scholar, IEEE, PubMed, and ScienceDirect between 1 January 2016 and 7 May 2022 using the following search terms: "schizophrenia", "automated detection of schizophrenia", "schizophrenia detection", "schizophrenia diagnosis", "deep learning", "mental health", "deep learning methods", "artificial intelligence", "machine learning", "prediction", "neural network". The above keywords were searched and shown results were downloaded. Those records with no reference of schizophrenia were discarded. Figure 2 depicts the process of selecting articles.

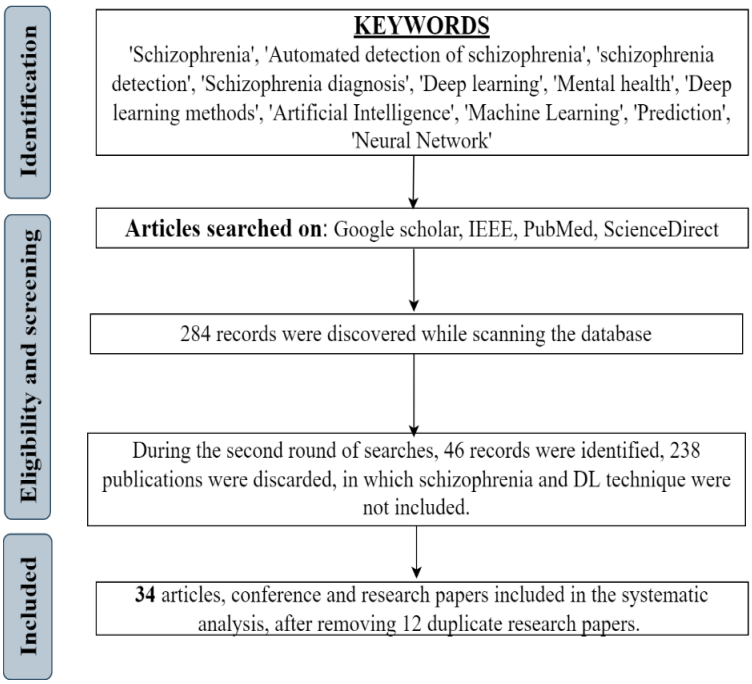

Figure 2. Literature search

3. Results

There were 34 studies, 25 involving DL methods (Table 1) and nine involving combined DL and ML methods (Table 2), included in this review, all of which reported binary classification results of SZ versus healthy controls (HCs). Most of the studies were based on MRI; in the latter, EEG studies predominated. In the first group, one study was based on the analysis of fundal retinal images [5]. This modality allowed direct visualization of blood vessels (and microvasculature) supplying the brain. All the studies were published from 2016 onwards, with the majority published in the last three years (Figure 3).

Table 1. Studies employing DL methods for detection of SZ.

Authors	Database	Subjects	Signal	DL Method	Accuracy
Oh 2019 [33]	IPN [34]	14 HC, 14 SZ	11-layer EEG	CNN	98.07%
Smith 2021 [35]	Kaggle datasets [36,37]	32 HC, 49 SZ	EEG	AlexNet ResNet50 VGG16 CNN	93.33% 93.34% 93.09% 93.36%
Phang 2019.[38]	Adolescents with symptoms of SZ [39]	39 HC, 45 SZ	EEG	1DCNN, 2DCNN	93.06%
Sridhar 2021 [40]	Private	25 HC, 15 SZ	EEG	LSTM	87%
Santo-Mayo 2016 [41]	Electro-Cap International from Eaton, Ohio, USA	31 HC, 16 SZ	EEG	MLP	93.42%

Aslan 2020 [6]	1. MHRC [42]; 2. IPN [34]	39 HC, 45 SZ; 14 HC, 14 SZ	2D EEG	CNN	95%; 97%
Chandran 2020 [43]	IPN [34]	14 HC, 14 SZ	EEG	LSTM	99.0%
Qureshi 2019 [18]	COBRE [44]	72 HC, 72 SZ	fMRI	3DCNN	98.09 ± 1.01%
Yang 2019 [45]	COBRE [44]; UCLA and WUSTL [46]	232 HC, 153 SZ	fMRI	Multiple feature image capsule network ensemble (MFIC)	82.83%
Campese 2019 [47]	Dataset-A; Dataset-B [47]	55 HC, 46 SZ; 122 HC, 54 SZ	sMRI	3DCNN (VNet)	83.13%; 71.63%
Niu 2019 [48]	Resting-state complex-valued fMRI [49]	40 HC, 42 SZ	fMRI	ICA-CNN	90%
Weizheng Yan 2019 [50]	Seven Hospitals [50]	542 HC, 558 SZ	fMRI	RNN	83·2% (multisite pooling), 80·2% (leave-one-site-out classification)
Qiu 2019 [51]	Resting-state complex-valued fMRI [49]	40 HC, 42 SZ	fMRI	CNN	91.32% (DMN), 98.75% (AUD networks)
Oh 2019 [52]	Chonbuk National University Hospital [52]	41 HC, 103 SZ	fMRI	3DCNN	84.29%
Pinaya 2016 [53,54]	Multisite [54]	83 HC,143 SZ	sMRI	DBN	73.6%
Patel 2016 [55]	COBRE [44]	72 HC, 72 SZ	fMRI	SAE	92%
Yan 2017 [56]	Multisite [54]	83 HC, 143 SZ	rs-fMRI	DNN	84.75%
Han 2017 [57]	Affiliated Hospital [57]	31 HC,39 SZ	rs-fMRI	DNN	79.3%
Dakka 2017 [58]	FBIRN [54]	169 HC, 135 SZ	4D-fMRI	RNN	63%
Latha 2019 [59]	COBRE [44]	72 HC,72 SZ	MRI	DBN	90%
Zeng 2018 [60]	Multiple datasets [60]	607 HC, 474 SZ	fc-MRI	DDAE	81%-85%
Matsubara 2019 [61]	Open fMRI [13]	122 HC, 50 SZ	rs-fMRI	DNN	76.6%

Srinivasagopalan 2019 [62]	COBRE [44]	72 HC, 72 SZ	sfMRI, fMRI	DNN	94.4%
Lin 2022 [63]	Complex-valued fMRI [49]	40 HC, 42 SZ	fMRI	3DCNN	96.04 ± 2.08%
Appaji 2022 [5]	NIMHANS [64]	188 HC, 139 SZ	Fundal images	CNN	95.0%

AUD, auditory cortex; COBRE, Center for Biomedical Research Excellence; DMN, default model network; FBIRN, functional biomedical informatics research network data repository; IPN, Institute of Psychiatry and Neurology; MHRC, Mental Health Research Center; NIMHANS, National Institute of Mental Health and Neurosciences; UCLA, University of California, Los Angles; WUSTL, Washington University in St. Louis.

Table 2. Studies employing combined DL and ML methods for the detection of SZ.

Authors	Database	Subjects	Signal	DL Method	Accuracy
Chu 2017 [65]	Shanghai Mental Health Center[65]	40 HC, 40 SZ (high risk), 40 SZ (first time)	EEG	CNN+Random forest	99.2% 81.6% (HR) 96.7% (FT)
Ahmedt-Aristizabal 2020 [7]	Private	40 HC, 65 SZ; 45 HC, 65 SZ; 57 HC, 65 SZ	EEG	CNN+LSTM	69.80%
Saeedi 2022 [66]	IPN [34]	14 HC, 14 SZ	1D EEG	CNN+FFT; CNN+Wavelet; CNN+LSTM	99.04% 98.32% -
Shoeibi 2021 [67]	IPN [34]	14 HC, 14 SZ	EEG	1DCNN+LSTM	99.25%
Sun 2021 [68]	Huilongguan Hospital	55 HC, 54 SZ	EEG	CNN+LSTM	99.22 %
Singh 2020 [8]	1. Adolescents with symptoms of SZ [39]; 2. IPN [34]	39 HC, 45 SZ (1); 14 HC, 14 SZ (2)	EEG	CNN+LSTM	94.08% (1); 98.56% (2)
Shalbaf 2020 [1]	IPN [34]	14 HC, 14 SZ	EEG	CWT, ResNet-18-SVM, 10-fold cross-validation	98.60%
Phang 2019 [69]	Adolescents with symptoms of SZ [39]	39 HC, 45 SZ	EEG	DNN-DBN	95%
Sundari 2021 [70]	COBRE [44]	20 HC, 20 SZ	fMRI	RNN-LSTM	81.3%

COBRE, Center for Biomedical Research Excellence; IPN, Institute of Psychiatry and Neurology

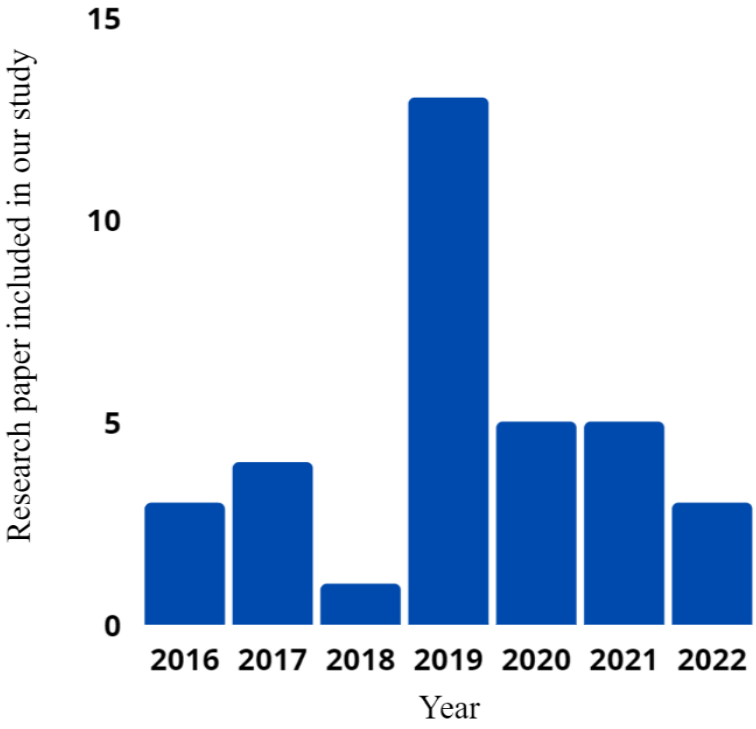

Figure 3. Distribution of reviewed studies by year of publication.

The databases that were used in the 34 studies are summarized in Table 3. They comprised predominantly EEG and MRI signal datasets of SZ patients and HCs. Among EEG datasets, the most commonly used was the Institute of Psychiatry and Neurology (IPN) from Warsaw, Poland, which contains 19-channel EEG signals from 14 patients with paranoid SZ and 14 HCs of both sexes with a mean age of approximately 27 to 28 years. The Kaggle Datasets [36,37] comprises EEGs of 81 subjects (49 SZ, 32 HCs; 67 male, 14 female; mean age 39 years) recorded when performing fundamental sensory tasks. The Electro-Cap International dataset from Eaton, Ohio, USA comprises 17-channel EEG-ERP data of 47 subjects (16 SZ, mean age of 36.33 ± 10.47 years; 31 HCs, mean age 29.85 ± 9.75 years). The larger Adolescents with Symptoms of SZ dataset [39] contains one-minute 16-channel resting-state EEG recordings acquired from 84 subjects (45 SZ, 39 HCs) by researchers at the Lomonosov Moscow State University. The Mental Health Research Center database [42] contains 16-channel EEG data from 84 young subjects (45 SZ, 39 HCs; mean age 12.25 years). The Shanghai Mental Health Center dataset [65] comprises 64-channel EEG acquired from 40 SZ patients characterized as high risk, 40 patients presenting with the first episode of SZ, and 40 HCs. The Huilongguan Hospital in Beijing, China acquired 60-channel EEG from 109 subjects (54 SZ, 55 HCs; mean age 41.00 ± 1.59) [68]. In a study using a private EEG dataset [7], five routes from the midline were analyzed: Fz, FCz, Cz, CPz, and Pz.

The Center for Biomedical Research Excellence (COBRE) dataset [44] comprises MRI images acquired from 72 HCs and 72 SZ patients who had been screened to be free from substance abuse problems or dependency in the previous 12 months. The resting-state complex-valued fMRI dataset [49] was obtained by performing 149 scans on 82 subjects (42-SZ, 40-HC). The Chonbuk National University Hospital comprises MRI acquired from 144 subjects (103 SZ, 41 HCs; age range 18 to 59 years). The Multisite MRI dataset in [54] was acquired from 226

individuals, 143 (95 male, 48 female; mean age 37.12 ± 10.99 years) of whom were SZ patients at an outpatient unit, and 83 were from a government job agency (mean age 35.49 ± 11.08 years).

The National Institute of Mental Health and Neurosciences (NIMHANS) dataset from Bengaluru, India, comprises fundal retinal photographic images of 327 subjects (139 SZ, 188 HCs; age range 18 to 50 years). The SZ patients had an average onset age of 24.9± 5.6 years, 7.9 ± 5.4 years of disease, and were in various phases of illness, with a mean Brief Psychiatric Rating Scale of 24.4 ± 9.4. UCLA dataset [46] was used by BO yang [45], which includes a total of 192 subjects (58 SZ and 134 HC), and the fMRI data were obtained from a 3 Tesla SIEMENS TIM scanner with a matrix size 64x64. And the WUSTL [46] dataset was also used by BO yang, and it includes total of 64 individuals (23 SZ, 41 HC). Takashi Matsubara [61] used the Open fMRI dataset, which consists of the fMRI data of 221 subjects (50 SZ, 122 HC and 49 patients with bipolar disorder). Another SZ dataset is from the Affiliated hospital of Xinxiang Medical University. This database consists of a total of 70 subjects (39 SZ, 31 HC), and the symptoms of patients were evaluated using the Positive and Negative Syndrome Scale.

The Seven Hospitals dataset is the largest. It comprises MRI data acquired from 1100 subjects (558 SZ, 542 HC; age range 18 to 45 years) recruited from seven different hospitals in China: Xinxiang Hospital GE, Xinxiang Hospital Siemens, Renmin Hospital, Beijing Huilongguan, Xijing Hospital, Zhumadian Psychiatric Hospital, and Peking University Sixth Hospital.

Database	**Subjects**	**Average age (years)**
EEG		
Institute of Psychiatry and Neurology [34,67]	14 HC (7 male, 7 female), 14 paranoid SZ (7 male, 7 female)	Male 26.8 ± 2.9, Female 28.7 ± 3.4 (HC), Male 27.9 ± 3.3, Female 28.3 ± 4.1 (SZ)
Kaggle [36,37]	32 HC, 49 SZ (67 male, 14 female)	39
Adolescents with Symptoms of SZ [39]	39 HC, 45 SZ	NR
Electro-Cap International [41]	31 HC, 16 SZ	29.85 ± 9.75 (HC), 36.33 ± 10.47 (SZ)
Mental Health Research Center	39 HC, 45 SZ	12.25
Shanghai Mental Health Center [65]	40 HC, 40 SZ (high risk), 40 SZ (first time)	NR
Huilongguan Hospital [68]	55 HC, 54 SZ	41.00 ± 1.59
MRI		
COBRE [44]	72 HC, 72 SZ	18 to 65
UCLA [46]	134 HC, 58 SZ	NR
WUSTL [46]	41 HC, 23 SZ	NR
Resting state-Complex value fMRI [49]	40 HC, 42 SZ	36.25 ± 11.40 (HC), 41.05 ±14.16 (SZ)
Seven Hospitals [50]	542 HC, 558 SZ	28.0±7.2(HC), 27.6±7.1(SZ)
Chonbuk National University Hospital [52]	41 HC, 103 SZ	32.46 ± 9.21
Multisite [54]	83 HC, 143 SZ	37.12 ± 10.99

Affiliated Hospital [57]	31 HC, 39 SZ	31
fBIRN [54]	169 HC, 135 SZ	18-21
Open fMRI [13]	122 HC, 50 SZ	NR
Fundal photography		
NIMHANS [64]	188 HC, 139 SZ	24.9 ± 5.6

COBRE, Center for Biomedical Research Excellence; NIMHANS, National Institute of Mental Health and Neurosciences

NR, not reported

Table 3. Demographics of SZ patients and healthy controls in the databases used in the reviewed studies.

Sr.no	Database	Database usage
1	Institute of Psychiatry and Neurology	7
2	Kaggle	1
3	Adolescents with Symptoms of SZ	3
4	Electro-Cap International	1
5	Mental Health Research Centre	1
6	Shanghai Mental Health Centre	1
7	Huilongguan Hospital	1
8	COBRE	7
9	UCLA	1
10	WUSTL	1
11	Resting state-Complex value fMRI	3
12	Seven Hospitals	1
13	Chonbuk National University Hospital	1
14	Multisite	2
15	fBIRN	1
16	Affiliated Hospitals	2
17	Open fMRI	1
18	National Institute of Mental Health and Neurosciences	1

Table 4. Database usage by researchers

4. DL algorithms for SZ detection

The most popular DL algorithms employed were convolutional neural network (CNN), deep neural network (DNN), and long short-term memory (LSTM); and several models used composite algorithms, e.g., CNN-LSTM, CNN-Wavelet, etc. (Tables 1 and 2). Detailed explanations of the various DL algorithms used in the reviewed studies are given below.

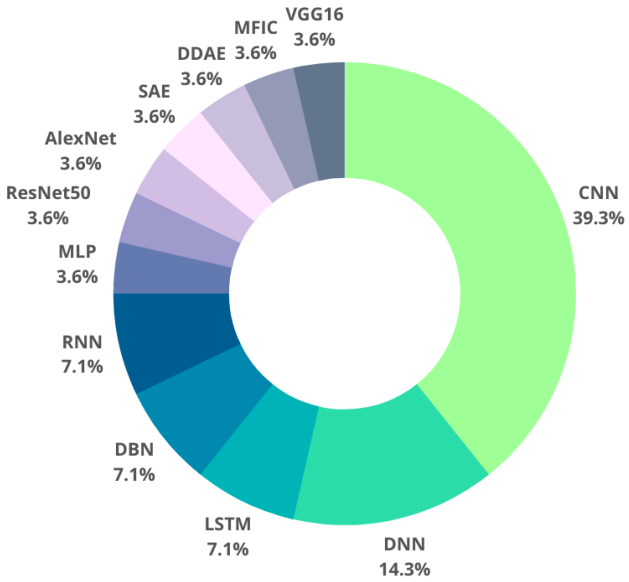

Figure 4. DL methods used by the researchers

To get over the drawbacks of feature extraction-based approaches, various researchers have advocated using convolutional neural networks (CNN) or a mix of time-frequency analysis and CNN for the automated identification of SZ. The CNN model is not only computationally efficient and fast, but also requires fewer learnable parameters. This is conclusive evidence that the CNN model outperformed the best available transfer learning methods. It is effective in learning and extracting abstractions of 2D features, and its structure is highly suited for processing 2D and 3D images [51]. Majority of the researchers are using CNN for classification between SZ and HC patients. Also, it is not always necessary that CNN is good because that depends on the number of layers, filters and the number of neurons selected. So, it cannot be primary conjecture. There are various possible variations of CNN also, that could be used like people have used transfer learning also. And as there are many hyperparameters that needs to be tuned, proper tuning of hyperparameters may produce a better CNN or proper tuning of LSTM may produce better results than the CNN. Apart from CNN, Deep neural network (DNN), Long short-term memory (LSTM), Deep Belief Networks (DBN), Recurrent Neural Network (RNN) are traditional DL algorithms that researchers commonly use.

It is analyzed that despite the Long Short-Term Memory (LSTM) based model providing the highest classification results (99% efficiency), convolution neural network (CNN)-based methods have been one of the most preferred DL techniques. It has been used by 11 researchers, followed by DNN techniques employed by four researchers, and two studies have used RNN, DBN, and LSTM. Multilayer perceptron [41], ResNet50 [35], AlexNet [35], stacked autoencoder [55], multiple feature image capsule (MFIC) network ensemble [45] and denoising autoencoder have

been used by different researchers. It is observed that LSTM-based models attained the maximum accuracy of 99% [43] and the average of accuracy attained by various LSTM-based models was found to be 93%. The CNN-based models attained the highest accuracy of 98.75% with an average of 91.76%. Hence, CNN-based, and LSTM-based models seem to be the most promising techniques for identifying SZ. Besides, it has been observed that the proper tunning of the hyper parameters of CNN or LSTM can lead to the development of accurate and efficient models for detecting SZ.

We have analyzed many CNN-based methods that have yielded promising classification performance. However, one of the LSTM-based models [43] provides marginally better accuracy than the best CNN-based model. It is to be noted that proper tuning of the hyperparameters of CNN, LSTM or bi-LSTM models can further improve the performance. For the future, we suggest developing DL-based models by training them with large databases instead of using transfer learning –based pre-trained networks VGG16, ResNet50, and AlexNet. In addition, various DL techniques such as generative adversarial network (GAN), autoencoder, bi-directional LSTM, Boltzmann machines, reinforcement learning, simple graphical models (SOM), and radial basis function neural networks (RBFN) can be explored for developing models to detect SZ.

Figure 5 shows the maximum accuracy achieved by various DL-based technique. It is seen from the bar graph the that maximum accuracy achieved by LSTM model is 99% and the CNN model has achieved comparable classification accuracy of 98.75%. There is no significant difference in the classification accuracy of CNN and LSTM models. It can also be observed that the trained models like ResNet50, AlexNet and VGG16 have also shown significant classification results of greater than 90%. And the RNN model has achieved significantly less classification accuracy of 83.2% as compared to other DL models.

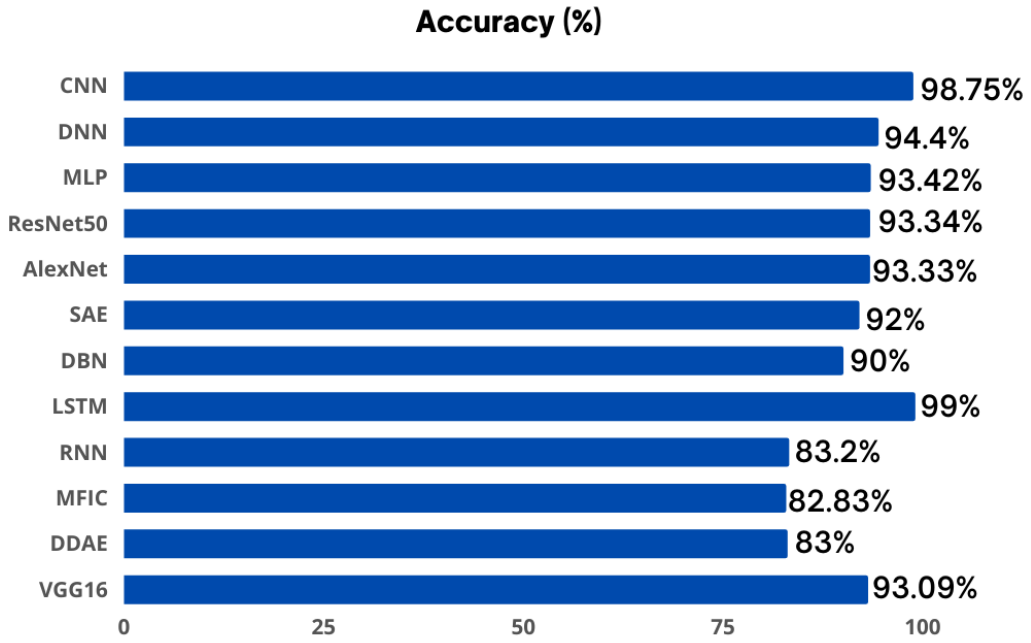

Figure 5. Maximum achieved accuracy by different DL models

DL Methods	Maximum accuracy (%)	Minimum accuracy (%)	Average accuracy (%)
CNN	98.75	71.63	91.76
DNN	94.4	76.6	83.76
DBN	90	73.65	81.8
LSTM	99	87	93
RNN	83.2	63	75.46
MLP	93.42	93.42	93.42
ResNet50	93.34	93.34	93.34
AlexNet	93.33	93.33	93.33
VGG16	93.09	93.09	93.09
DDAE	83	83	83
SAE	92	92	92
Multiple Feature Imaging Capsule	82.83	82.83	82.83

Table 5. Maximum, minimum and average accuracy achieved by various DL techniques.

4.1. Convolutional neural network

A CNN consists of an output layer and an input layer, with hidden layers in between [71]. In contrast to traditional neural networks, the neurons in a CNN's layers are organized in three dimensions: width, depth, and height. The building blocks of CNNs are convolution, normalizing, pooling, and Fully Connected (FC) layers (Figure 6). CNNs filter input volumes to higher levels of abstraction by employing several convolution layers. The convolution function builds feature maps for the following layer by extracting features from input signals [72].

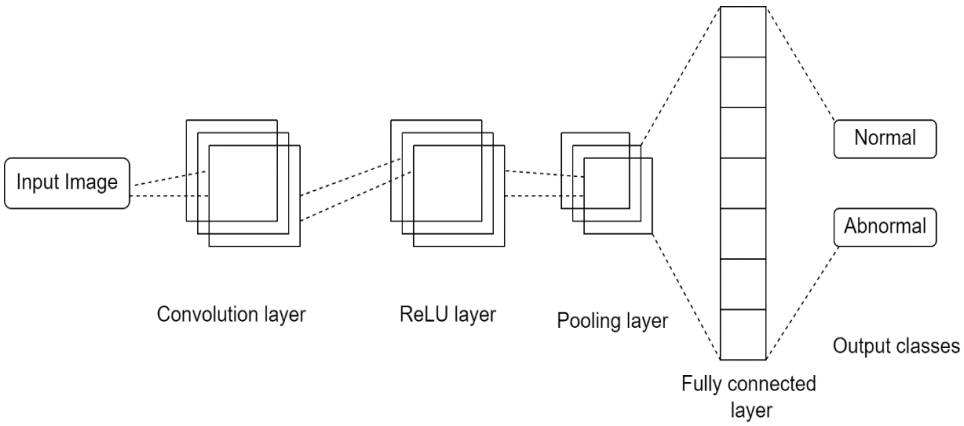

Figure 6. Schema of a Convolution Neural Network.

The batch data normalization layer is applied to the training data between the intermediate layers to normalize them, which accelerates and strengthens the learning process. Max pooling minimizes the size of the feature map by calculating and letting through only the highest value for each kernel. Based on the training dataset and the problem, the FC layer splits the data into numerous categories. Every neuron of the FC layer is coupled to every neuron in the max-pooling layer, and the output reliably predicts if the input signal is normal or pathological [73,74]. The output of the max-pooling layer contains the most prominent features of the previous features.

1. Convolution layer. This initial layer is used to extract different attributes from the input images (Figure 6). The image in the form of a matrix of dimension N x N pixels is input to the convolution layer, where it is convolved using a small matrix, the convolution filter, which is also known as kernel [75]. The kernel extracts features from the image [75] based on a set of values or discrete numbers known as the kernel weight. The convolution filter is superimposed on the input image matrix [75], and its dot product is computed and summed to obtain a single scalar result [75]. The operation is repeated as the filter is moved horizontally from left to right and vertically from top to bottom in stepwise order over the entire image matrix until all possible positions have been covered [73]; the stride is the number of pixels the filter is moved at a time. The generated summed dot product values constitute the output's feature map, which contains image data such as corners and edges [75]. This feature map is passed on to the subsequent layers, which acquire various characteristics from this input. This process is repeated at every convolution layer in the network: with every training, the convolution layers are updated [44,75] and learned to extract essential information [73,44].

2. Pooling layer. Pooling is carried out after the convolution procedure to sub-sample the large-sized feature map to reduce its dimensionality [29] while retaining the most critical information (Figure 6). There are different pooling functions: global max pooling, tree pooling, global average pooling, gated pooling, max pooling, average pooling, and min pooling [75]. Similar to the convolution procedure, the size of the pooling layer kernel (typically smaller than the convolution layer kernel) and stride size are pre-assigned. The output of the pooling function contains information on the existence and the location of a specific

feature in the input image [75,76]. The granularity of the information deteriorates as the size of the pooling layer kernel or stride increases [75].

3. Fully connected layer. A FC layer is placed at the end of every CNN architecture to perform the task of final classification (Figure 6). Akin to a multilayer perceptron (MLP) network, numerous FC layers can be linked in sequence to perform mathematical computations. Every neuron in the FC layer is coupled to every neuron in the preceding layer [74,76]. Typically, the pooling layer's output feature map is fed to the FC layer in the form of a vector, which has previously been optimized [75]. The FC layer's output is the overall output of the CNN architecture.

4. Dropout. Overfitting can arise if all features are utilized to connect neurons in the CNN architecture [72,75]. To avert this, random neurons are dropped at every epoch [73] that are no longer used in forward- or back-propagation [75]. For example, when a dropout of 0.25 is specified, 25% of the nodes in the neural network are dropped at random [73]. This ensures that the model can learn independent features during training updates.

5. Activation function. This can learn and estimate any complicated link between neurons [73], i.e., nonlinear input and output mapping. The activation function generates the appropriate output result using the weighted sum of neuron input and bias as the input value [75]. Back-propagation during model training provides the capacity to discriminate and learn complicated objects [75]. There are various types of activation functions, including:

• Sigmoid, a S-shaped figure [75] that yields an output between 1 and 0 when the input is a real value

$$\boldsymbol{f(\theta)_{sigmoid}} = \frac{\mathbf{1}}{\mathbf{1}+\boldsymbol{e^{-\theta}}}$$

• Tanh, which yields an output between 1 and -1 [75] when the input value is real.

$$\boldsymbol{f(\theta)_{tanh}} = \frac{\boldsymbol{e^{\theta}} - \boldsymbol{e^{-\theta}}}{\boldsymbol{e^{\theta}}+\boldsymbol{e^{-\theta}}}$$

• Rectified linear unit (ReLU) converts the complete set of inputs to positive values, effectively reducing the computation demand [74-76]. It is often used in CNN architecture (Figure 4).

$$\boldsymbol{f(\theta)_{ReLU}} = \boldsymbol{max}(\mathbf{0}, \boldsymbol{\theta})$$

Other activation functions, which are modified versions of the above, including Leaky ReLU, Noisy ReLU, and parametric linear units [75], may be deployed according to the model

4.2. One-dimensional convolution neural network

The most typical applications for one-dimensional (1D) CNN is text and 1D signals. For example, CNN and regulation algorithms are used to classify 12-lead electrocardiography signals [72,73]. In 1DCNNs, there are two layers: (1) CNN layers, which include both 1D convolutions and sub-sampling, and (2) MLP layers, which are the hidden and output layers of a conventional MLP. For categorization by MLP layers, the CNN layers learn to extract features by evaluating raw data [77]. As a result, the feature extraction and classification methods are combined into a single entity that may be adjusted to enhance classification results [71,74]. This is the primary benefit of CNNs, which may also deliver minimal computational complexity. Phang et al. [38] developed a novel deep CNN

architecture and the accuracy achieved by this model is 93.06%, the multi-domain connectome CNN (MDC-CNN) integrates time-domain, frequency-domain, and topological measures of brain connectivity networks. In other studies, the convolutional architecture was based on one type of connectivity measure from a single domain, like the Pearson correlation for functional connectivity, which doesn't consider the direction of connections or how the brain networks are set up. For the first time, Phang et al. used effective brain connectivity, a generalization of FC that considers the direction of information flow between brain regions, to automatically tell SZ apart using CNN. They considered different measures of directed connectivity, estimated from EEG to get a sense of how the brain network organization is messed up in SZ.

4.3. Two-dimensional convolution neural network

Two-dimensional (2D) CNN is composed of four convolution blocks, each with two convolution layers and filter sizes of 5 x 5 for the first unit and 3 x 3 for the following blocks, as well as ReLU activation functions [78]. Batch normalization is not employed. The first block consists of 16 filters, with doubled quantities in each subsequent block. The second convolution layer in each block is created by down-sampling with a stride of 2. After the final convolution layer, and before being fully connected to two FC layers with ReLU activation levels of 256 and 64, respectively, a fattening technique and a dropout layer (p=0.3) are implemented [78].As a result, Aslan and Akin [6] achieved a maximum 97% efficiency using 2DCNN on EEG signals for the binary classification of SZ versus HC.

4.4. Three-dimensional convolution neural network

This is typically used for volumetric data. 3D convolution filters [79] scan over the voxels and conduct convolutional operations to build the feature map based on the dot product of individual tensors. Each filter's weights and biases are trained to recover the important attributes from the input. Common hyperparameters used to create convolutional methods include padding, stride, and filter size [80]. As mentioned before, the stride parameter sets the size of the step that the filter takes every time it moves. Padding the inputs with zero-value voxels is necessary to maintain the sparsity of output. The maximum or average value inside a volume can be determined using pooling techniques. Activating layers are utilized to give the CNN nonlinearity by applying element-wise nonlinear changes to the input tensor. At the end of the 3DCNN, FC layers are deployed to connect neurons from two adjacent layers [81]: taking the preceding hidden layer's flattened tensor as input and mapping it to the predicted result. The FC layer's weights and biases are also 3DCNN trainable parameters. The loss function is defined as the mean square error between 3DCNN prediction and the classification algorithm of the training dataset [82]. Qureshi et al. [18] applied 3DCNN on fMRI signals and attained 98.09 ± 1.01% accuracy for SZ detection. Similarly, Campese et al. [47] applied a 3DCNN model on a sMRI dataset and attained 83.13±9.05% accuracy for SZ detection.

4.5. Long short-term memory

LSTM [83,84] is a recurrent neural network (RNN) form. It contains feedback connections, in contrast to standard feed-forward artificial neural networks, allowing it to analyze whole data sequences (e.g., audio or video data) [85], not only individual data points. It has been applied to unsegmented robot control, machine translation, and healthcare applications [4]. A LSTM unit comprises a cell, an input gate, an output gate, and a forget gate [86,87]. The three gates control the flow of data to and from the cell, while the cell maintains values for several time frames. LSTMs were created to address the problem of vanishing gradients that can occur while training regular RNNs [87,88] and are well suited for analyzing and categorizing time series data. For example, using LSTM to classify EEG signals for SZ detection, Chandran et al. [43] used LSTM method to classify EEG signals for SZ detection and it provided 99.0% accuracy. When they performed their study, not much work was done on EEG signals using LSTM except for predicting depression and epileptic seizures. And they noticed that LSTM is prominent by its feedback connections unlike observed in standard neural networks and is therefore preferred when working with

time series data. As a subset of RNN, LSTM networks excel at discovering and labelling features in huge datasets. An extremely high percentage of classification accuracy is achieved in classifying EEG signals by selecting the proper pre-processing methods, the number of inputs, hidden and output layers, nodes in each layer, scaling factor (α), and cross-validation framework.

4.6. AlexNet

AlexNet is a CNN network that has been trained to sort 1.2 million images into 1,000 distinct categories. It outperformed state-of-the-art algorithms at the time, with top-1 and top-5 error rates of 37.5 % and 17%, respectively, in the ImageNet competition of 2010 [35]. It contains eight layers: five convolution layers with a combination of max pooling followed by three fully connected layers [35]. This network can be trained on a large number of graphics processing units. For example, Smith et al. [35] used AlexNet to classify EEG signals and attained 93.33% accuracy for SZ detection.

4.7. Multilayer perceptron

An MLP is a feed-forward neural network-based network augmentation [41] that contains three types of layers: input, hidden, and output layers. The input layer receives and processes the input signal, while the output layer handles prediction and categorization. In an MLP, data flows from the input to the output layer, similar to a feed-forward network [41]. Back-propagation learning is used to train the neurons in the MLP. The most common applications of MLP are pattern classification, identification, forecasting, and estimation. Santos Mayo et al. [41] applied MLP classification to EEG signals and attained 93.42% accuracy for SZ detection.

4.8. Recurrent neural network

In RNNs, every time step is represented by a fixed activation function unit [70] containing a hidden internal state. This hidden state represents the network's historical knowledge at any given time step. RNN converts independent action potentials into interdependent activations by applying the same weights and biases to all layers, minimizing the intricacy of increasing parameters, and memorizing each prior output by passing that on to the next hidden level [70]. Dakka et al. [58] applied the RNN classification method on 4D fMRI signals and attained 63% accuracy for SZ detection.

4.9. ResNet50

ResNet is available in several variants, all with the same core components but with variable layer thicknesses. Resnet50 is a widely used variant with 50 neural network layers [89] —48 convolution layers, one max pooling layer, one average pooling [90] —and 3.8 x 109 floating-point operations. Smith [35] applied ResNet50-based classification to EEG signals and attained 93.34% accuracy in detecting SZ.

4.10. VGG16

VGG16 is a CNN architecture with a fixed configuration: 16 weighted layers comprising convolution layers with 3 x 3 filters (stride 1), constant padding, and a max-pooling layer with 2 x 2 filters (stride 2) [91]. With an estimated 138 million parameters, the network is rather large [91], but the hyperparameters are comparatively low because of the stable architecture using convolution layers of 3x3. The most noticeable change, when compared to older deep learning systems, is the incorporation of a deeper learning architecture. Smith et al. [35] used the available VGG16 transfer learning technique to classify EEG signals and attained 93.0% accuracy for detecting SZ. The VGG16 network is fed with images up to 224 × 224 × 3 (RGB). General approaches such as conventional machine learning methods (SVM, RF, LDA, KNN) require multiple tuning of parameters for decomposition, feature extraction, and

classification and the empirical selection of these tuning parameters may cause information loss and increased misclassification but the proposed method by Smith involve the identification of SZ by separation of rhythms, extraction of features (time, frequency, entropy, spectral, and nonlinear), and classification. Their model proposes the spectrograms, scalograms, and smoothed pseudo-Wigner-Ville distribution (SPWVD) based time-frequency representation (TFR) using CNNs for SZ detection. The limitations of our developed model are that it employed empirical selection of parameters and the memory requirements are more compared to feature extraction and classification techniques.

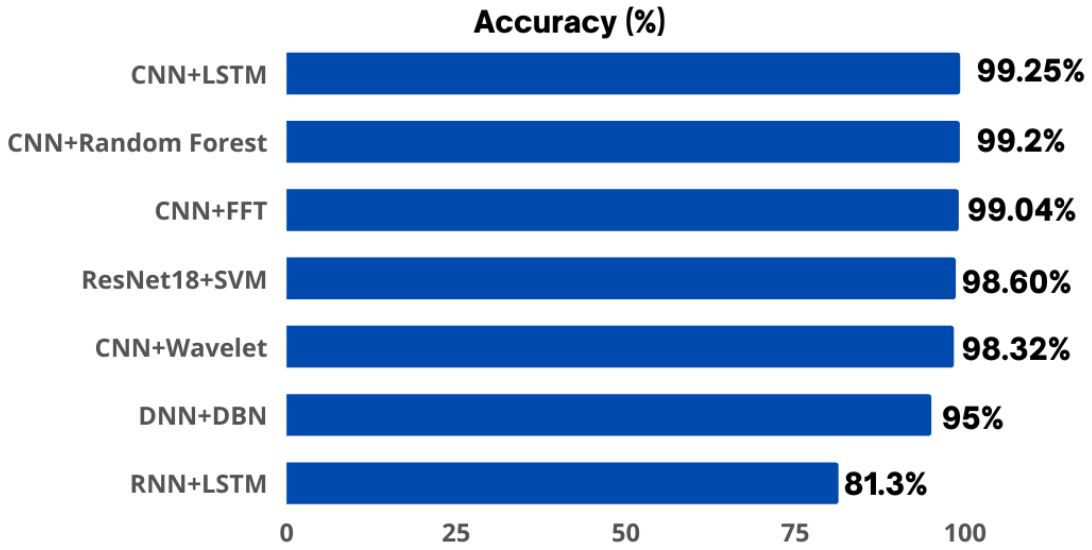

Figure 7. Maximum classification accuracy achieved by combining ML and DL models

Figure 7 shows the accuracies achieved by the various models that are obtained by combining different DL and ML models. From the bar graph, it is seen that CNN+LSTM model has achieved maximum classification accuracy of 99.25% and RNN+LSTM model has significantly less classification accuracy of 81.3%. Other than RNN+LSTM, there is no significant change in the classification accuracy of other composite DL models reviewed in our study.

4.11. CNN+LSTM

CNN-LSTM comprises a series of convolutional layers followed by some LSTM layers [7]. The former extracts rich information from input data, which are fed to the latter to extract temporal information [66]. Finally, FC layers are applied to the temporal information to complete the classification [66]. Ahmedt-Aristizabal [7] used the composite CNN+LSTM classifier method and attained 69.80% accuracy in detecting SZ using EEG signals.

4.12. CNN+Random Forest

This is a random forest (RF) classifier [65] with a modified CNN. To generate RF, a training set is utilized:

$$(\boldsymbol{a_h}, \boldsymbol{y_h})_{\boldsymbol{h=1}}^{\boldsymbol{n}}$$

where ‘a’ and y are data features and labels, respectively. This generates predictions ˆy for new points á by studying the point’s surroundings, which is defined by a weight function Hl in the lth tree [65]:

$$\hat{y}_l = \sum_{h=1}^{n} H_l(a_h, a')y_h$$

where Hl (ah, a') is the non-negative weight of the hth training point with respect to the new point; and n, the number of nodes in the next layer [65]. Estimating a set of M trees with distinct weight functions is averaged. The predictions are given as [65]:

$$\hat{y} = \sum_{l=1}^{M} \sum_{h=1}^{n} H_l(a_h, a')y_h$$

where the predicted class is:

$$\hat{p}_\iota = argmaxy$$

Chu et al. [65] suggested a method in which they extract features using CNN and classify them with Random Forest and attained 96.7% accuracy for diagnosing SZ. Previous studies have failed to obtain accurate and robust classification results using single-channel or multi-channel EEG fragments, making them unsuitable for practice. In their study, instead of using short-term EEG data, which was proven to be insufficient for individual recognition in schizophrenia (IRS) analysis, they used streaming EEG data obtained by multi-channel scalp electrodes. A voting layer was built on top of the employed neural networks to address the classification challenge. The results of their experiment show that the performance of classification would improve as the size of the training and data database grew.

4.13. RNN+LSTM

Conventional RNNs suffer from dual problems of vanishing gradients and exploding gradients in long sequences, which result in no actual learning and model instability, respectively. By incorporating memory cells of a LSTM network, this problem may be solved. Each LSTM unit remembers the preceding information [70]. Accordingly, the three inputs to each unit of the LSTM network—past output, current input, and previous memory—decides that single unit's output (Figure 8). The operations are given as:

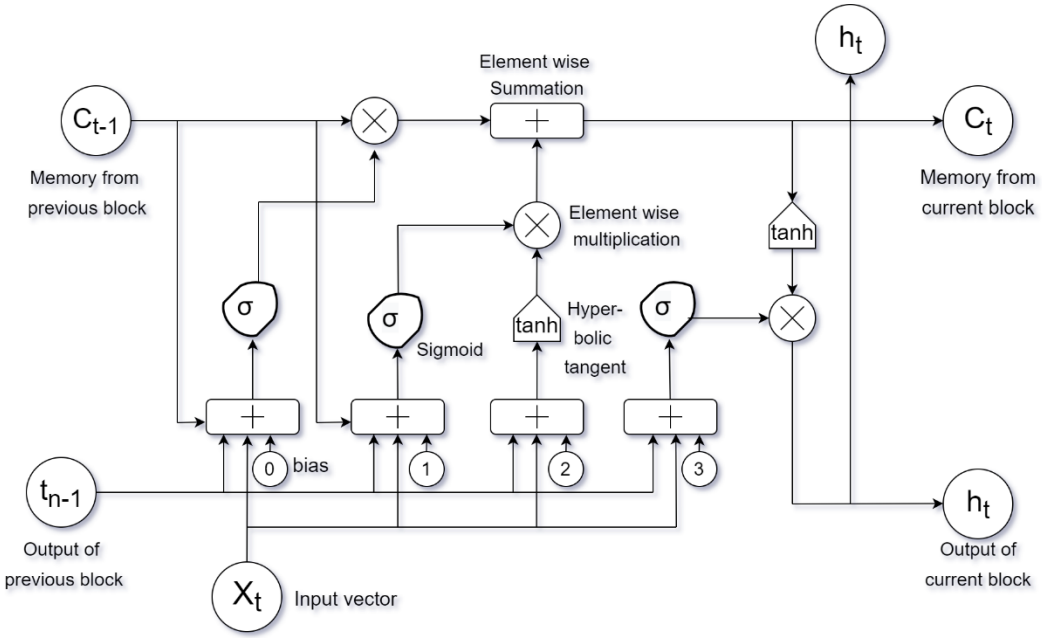

Figure 8. Architecture of a LSTM unit.

where σ represents the activation function, sigmoid; X_t, the input of the current time step; H_{t1}, the previous unit's output; C_{t-1}, prior unit's memory; C_t, the current unit's memory; H_{t-1}, the current unit's output.

$$I_t = \sigma(w_i[H_{t-1}, x_t] + b_i)$$

$$F_t = \sigma\big(w_f[H_{t-1}, x_t] + b_f\big)$$

$$O_t = \sigma(w_o[H_{t-1}, x_t] + b_o)$$

$$C_t = tanh(w_c[H_{t-1}, x_t] + b_c)$$

$$c_t = F_t * c_{t-1} + I_t * C_t$$

$$H_t = O_t * tanh(c_t)$$

FMRI analysis primarily employs spatial maps and connection patterns, rather than temporal details. Sundary et al [70] aimed to employ an LSTM deep learning model trained on fMRI time series collected from regions of interest (ROIs) to detect schizophrenia. As a result of its superior ability to characterize sequence data segments, LSTM-based RNN networks using ROI time series may be a useful tool in the detection of schizophrenia. In his work, the model is trained using a rather limited data set. Sundary et al. [70] provided an RNN-based LSTM model using regions of interest (ROI) based time series extraction and achieved an accuracy of 81.3%. And this model can characterize fragments of sequential data and can be a promising aspect in the identification of schizophrenia. Previous researchers haven't investigated how ROI time courses or seed time courses can be analysed with LSTM yet. Bidirectional LSTM is used in the network to run the input in both directions. This gave the network information from both the past and the future, which helped it work better. Because LSTM has both long-term and short-term memory cells, it doesn't have the problem of vanishing gradient in long sequence data, which is a problem faced by RNNs. So, LSTM is able to remember important pieces of sequential data important for learning. In the study, a small number of samples are used for training the model. The model's performance can further be improved by training with a greater number of samples.

4.14. ResNet18-SVM

In [1], the EEG data were segregated into five brain areas: frontal, central, parietal, temporal, and occipital lobes. The employed Resnet-18-support vector machine (SVM) model used average accuracy, sensitivity, and specificity values for scalogram pictures of the five designated brain areas to detect SZ. To boost classification performance, the brain areas were combined [1] The convolution layers in ResNet-18 are thinner [1], with numerous layered identity maps and shortcuts in the residual units [33]. Data-driven feature extraction and classification are both automatable processes for deep learning systems. These techniques simulate how the human brain processes information and creates decisions-making habits. Shalbaf et al. [1] introduced a method based on transfer learning and deep convolutional neural networks (CNNs) for diagnosing SZ patients from healthy controls. Their research offers a general way to model brain dysfunction by combining continuous wavelet transform (CWT), and transfer learning with four popular pre-trained deep CNNs (AlexNet, ResNet-18, VGG-19, and Inception-v3). This method first converts EEG signals into images using a continuous wavelet transform (CWT). Then, they are given to the popular models that are already trained: AlexNet, ResNet-18, VGG-19, and Inception-v3. It showed that combining the frontal, central, parietal, and occipital regions with the ResNet-18 produced the best results, with accuracy, sensitivity, and specificity values of 98.60%, 99.65%, and 96.92%, respectively.

4.15. 2DFFT-CNN

In [66], a 19-layer 2DFFT-CNN model combining 2D fast Fourier transform (FFT) operation and CNN was developed. To extract features from photos and minimize their size, two convolution procedures were followed by max-pooling layers, after which a dropout layer was implemented to limit the possibility of overfitting [66]. The max-pooling method was used once more after the convolutions to obtain Layer 8. Three further alternating convolution and dropout processes were conducted to create Layers 9 to 15. Next, the data were transformed via a flattening layer to a one-dimensional array, fed to a dropout layer connected to a dense layer with 32 units [66]. Two output neurons in the last dense (classification) layer displayed normal and SZ results.

4.16. 2DWavelet-CNN

In [66], a model was developed in which the first layer's output was generated using a two-dimensional Gabor wavelet transform [66]. The rest of the structure is the same as the 2DFFT-CNN structure. The Gabor filter is a linear texture analysis filter used in image processing that searches for specified frequency content in certain directions in a constrained zone surrounding the assessment point or region in the image [66]. A 2D Gabor filter is a Gaussian kernel function produced in the spatial domain by a sinusoidal plane wave [66].

5. Discussion

5.1. Classification and Detection

To identify SZ automatically via EEG inputs, Oh et al. [33] presented an 11-layer CNN model that was trained on data from the IPN database [34]. The model attained accuracy rates of 98.07% and 81.26% for non-subject and subject-based testing, respectively. Smith et al. [35] combined CNN with time-frequency analysis to overcome the shortcomings of feature extraction-based techniques for automated SZ detection. Scalograms, spectrograms, and smoothing pseudo-Wigner-Ville distribution (SPWVD)-based time-frequency representations (TFRs) were obtained using transformation techniques short-time Fourier transform (STFT), continuous wavelet transforms (CWT), and SPWVD, respectively. The 2D plots were then sent to pre-trained ResNet50, CNN, AlexNet, and VGG16. Using data from the Kaggle database [37], the composite SPWVD-based TFR and CNN model attained 93.36% accuracy. Phang et al. [38] developed a deep framework for SZ detection using EEG-derived brain connectomes that were based on a parallel ensemble of 1D and 2D CNNs. The unique multi-domain connectome CNN model was able to conglomerate information from many domains and dimensions using separate fusion methods. On the public Lomonosov Moscow State University Adolescents with Symptoms of SZ dataset [39], the model attained best-modified accuracy of 93.06% using decision-level fusion. Sridhar et al. [40] used LSTM to extract characteristic features and perform classification using a private EEG dataset, which comprised signals from fp1 and fp2 of a 10/20 electrode setup of 25 HC [92] and 15 SZ participants [93]. A two-layer LSTM with Adam optimizer yielded optimum accuracy of 87%. Santos-Mayo et al. [41] used the Neural Network MATLAB Toolbox (MathWorks Inc., Natick, Mass., USA) to build a MLP classifier that contains only one hidden layer, in which the neuron size could be adjusted from 5 to 30 to optimize the correct classification rate for each feature grouping under consideration. The 47 subjects (16 SZ, 31 HC) of Electro-Cap International were randomly assigned to three groups of 5, 28, and 14 in the validation, training, and test sets, respectively. Weights of the neural network were determined at random. This advanced supervised ML strategy was based on the well-known scaled conjugate gradient algorithm and used as the training performance metric, the square error. The model attained 93.42% accuracy. Aslan and Akin [6] used 2D time-frequency transformation in their VGG16-based CNN model. They trained the model on two

datasets—Mental Health Research Center database (45 SZ, 39 HC) [42] and IPN (14 SZ, 14 HC) [34] - and attained 95% and 97% accuracy results, respectively, for SZ detection. The CNN extracted informative features from the 2D scalogram images: these embodied spatial characteristics at the time-frequency level that produced significant variances with algorithm processing. CNN network visualization methods—gradient-weighted class activation mapping, saliency map, and activation maximization—were used to generate image outputs that contextualized the differences between SZ and HC, rendering the results more relatable to clinical end-users. Appaji et al. [5] employed a pre-trained CNN to identify SZ using fundal photographic images of the retina. On the 327-subject NIMHANS dataset, the model attained 95% accuracy and an area-under-curve of 0.98 for diagnosis of SZ vs. HC.

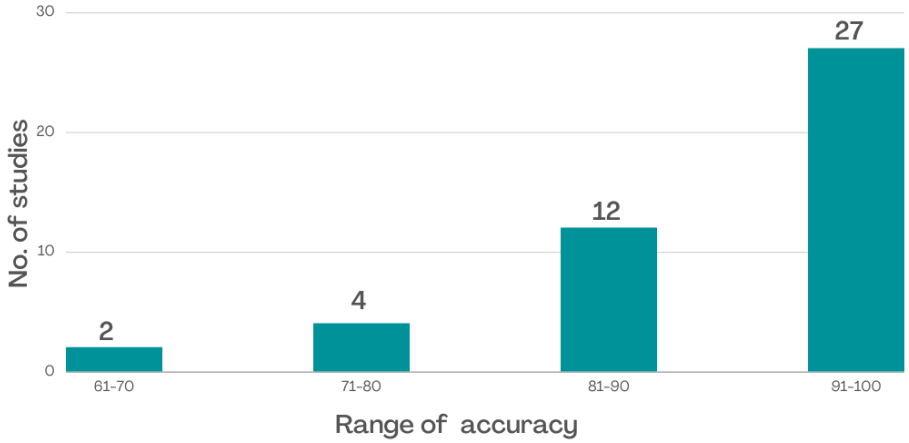

Figure 9. Section-wise accuracy achieved by the researchers; Maximum accuracies achieved are in the range of 91-100% by 27 researchers. Minimum accuracies are in the range of 61-70% achieved by 2 researchers. Also, the mean, median, mode of the accuracies of the studies reviewed in our study were found to be 89.72%, 93.33% and 95%, respectively.

Many researchers used deterministic finite automata and their modifications to categorize and detect patients with SZ by considering other brain regions of interest [4] on sMRI. Campese et al. [47] evaluated the effectiveness of conventional SVM, 2D, and 3D CNN on four neuroimaging tasks and observed that linear SVM outperformed 2D networks while the 3D structure outperformed the other two. sMRI signals from two separate datasets were used, and the most discriminative area-under-curve of 83.13 ± 9.05% was attained using VNet 3DCNN. Pinaya et al. [53,54] developed a deep belief network-based model for detecting SZ on sMRI and attained 73.6% accuracy on the Multisite dataset [54]. In their 3DCNN architecture model, Qureshi et al. [18] used the Oxford Centre for Functional Magnetic Resonance Imaging of the Brain Software Library (FMRIB Software Library, or FSL) tool MELODIC (multivariate exploratory linear optimized decomposition into independent components), which is based on independent component analysis (ICA), to separate noise and artifacts in resting-state fMRI data of the 144-subject COBRE dataset [44]. Using ten-fold cross-validation, the CNN model attained overall classification accuracy of 98.09 ± 1.01% (p 0.001). Yang et al. [45] employed a deep capsule network architecture for multiple feature extraction and a weighted classifier to enhance the classification process. By using the UCLA [46], WUSTL [46], and COBRE [44] fMRI datasets, they attained a classification accuracy of 82.83 %. Niu et al. [48] developed an ICA-CNN framework to address the issue of subject shortage for fMRI data. On resting-state complex-valued fMRI data from 82 participants (42 SZ, 40 HC) [49], the model attained an average accuracy of more than 90%. Yan et al. [50] developed a novel multi-scale RNN model to analyze fMRI time courses, which was the first effort at such categorization. On a large fMRI dataset (558 SZ, 542 HC) acquired from seven hospitals, the model attained 83.3 % and 80.2% accuracy rates using multi-site pooling and leaving-one-site-out classification strategies, respectively.

In our review of the last decade, there are no DL studies on the classification of pMRI and dMRI images. Ingalhalikar et al. [94] used pMRI data from 64 subjects and achieved 90.62% prediction on their nonlinear SVM-

based ML model. Caprihan et al. [95] attained 100% prediction using data from pMRI and dMRI scans with their dimensionality reduction ML method.

In our review, several studies employed combined DL and ML models. Chu et al. [65] substituted a random forest classifier for the SoftMax layer of the CNN model. By adding a vote layer on top of the developed neural network, they obtained a slight but consistently superior performance for the categorization of EEG data. The model attained 81.6%, 96.7%, and 99.2% for high-risk SZ, clinically stable first-episode SZ, and HC, respectively. Ahmedt-Aristizabal et al. [7] studied the evolution of aberrant traits in children who were first screened for SZ susceptibility at 9 to 12 and followed up for four years. The brain's response to deviant stimuli in a passive auditory oddball paradigm [96] was recorded on EEGs for all subjects. The performance of traditional ML approaches that rely on classification with raw data was compared with end-to-end DL approaches. Their recurrent deep CNN model attained 69.80 % accuracy, outperforming traditional sequence-modelling ML algorithms, using average cross-validation performance measurements. Sundari and Sujatha [70] used pre-processed fMRI to collect meantime data for 116 automated anatomical labelling atlas regions of interest. The data were spatially normalized and then smoothed with an 8 mm full-width at half-maximum Gaussian kernel before being fed to LSTM blocks. Using resting-state fMRI data of 20 subjects each of normal and SZ from the COBRE dataset, the temporal moment feature input yield was achieved with a maximum accuracy of 81.3%. Saeedi et al. used the gramian angular field to depict EEG data as various types of visuals, including gramian angular summation field and gramian angular difference field. Three models were studied: CNN-LSTM and two bespoke CNN architectures incorporating 2DFFT layers (CNN-FFT) and wavelet transform layers (CNN-Wavelet). Using the IPN dataset [34], CNN-FFT attained a maximum accuracy of 99.04%. Using EEG data from the IPN database [34], Shoeibi et al. [67] split the EEG waves into 25-second time frames and normalized them using Z-score or the norm L2. Three classification models were studied: LSTM, 1DCNN, and 1DCNN-LSTM. The latter attained 99.25 % accuracy for SZ detection, which outperformed the other two DL models. Shalbaf et al. [1] used continuous wavelet transform to convert EEG data into images, which were input to four pre-trained CNNs: Inception-v3, VGG-19, ResNet-18, and AlexNet, the outputs of which were fed to a SVM classifier. Using the IPN database [34], the model attained accuracy, sensitivity, and specificity of 98.60 ± 2.29 %, 99.65 ± 2.35 %, and 96.92 ± 2.25 %, respectively. The frontal, central, parietal, and occipital regions paired with the ResNet-18-SVM generated the best results. In [68], the EEG time series were normalized and converted into a sequence of red–green–blue graphics that contained spatial information. These were input to a hybrid deep neural network comprising CNN and LSTM. Using the Huilongguan dataset, the model yielded accuracy rates of 99.22% and 96.34% using FuzzyEn and FFT, respectively. Singh et al. [8] analyzed the spectral characteristics of EEG signals, which were categorized into distinct spectral subbands: delta, theta, alpha, beta, and gamma. For classification, raw temporal and spectral EEG segments were input to CNN models; and spectral information, a LSTM model. Adolescents with symptoms of SZ [39] and IPN datasets [34] attained classification accuracy rates of 94.08 % and 98.56 %, respectively.

There is little understanding of how organizations/clinics/hospitals use these methods in practice. Explainable machine learning could help us understand how a model works by using things like feature importance scores, counterfactual explanations, or training data is important [124]. Machine learning (ML) models are being used more and more in areas like healthcare, finance, and social media that people use daily [125]. Researchers have come up with many ways to explain to ML models so that people can trust them. Explanations can take many forms, such as telling a patient what symptoms point to a certain diagnosis or helping factory workers figure out where there are problems in a production line. Explainability techniques try to give direct transparency to human users by explaining how a model make a decision. This is often done to make the model more trustworthy [123].

5.2 Future trends –

- The main motivation of the study is to compare different DL models, Datasets used by the researchers for the classification of SZ. Based on our study, it can be suggested that CNN and

LSTM-based DL models provides efficient results. ML and DL are popular techniques and provided efficient models but still there is a requirement for an accurate and simple system that can be used in clinical setup or as handy or wearable compact devices.

- In our study, we have found that most of the researchers have used only a single dataset for the development of their models, further, the biggest dataset for the detection of SZ has been used by Yan et al. [50] which also contains 1100 subjects collected from seven various hospitals [50], and the smallest dataset provided by Institute of Psychiatry and Neurology [34,67], which contains 28 subjects and has been used in 7 studies. Based on our analysis, it is advisable that a mixed dataset can be used by collecting data from multiple sources. This dataset can be used to develop a robust model. Also, researchers should use bigger datasets to train different DL models.
- Most of the studies nowadays are based on the algorithms developed by combining different DL and ML methods. So, in the future new combinations of various DL or ML methods can be explored to provide more efficient results.
- CNN is a widely used in most of studies. It is suggested that the accuracy of the model may further be increased by combining it with other DL and ML algorithms.
- The maximum accuracy of 98% is achieved by CNN, and 99% using LSTM. Classification accuracy may be further increased by combining CNN with LSTM model. Shoebi et al. [67] achieved an accuracy of 99.25% by using this method.
- In addition, various DL techniques such as bi-directional LSTM, Boltzmann machines, reinforcement learning, generative adversarial network (GAN), autoencoder, simple graphical models (SOM), and radial basis function neural networks (RBFN) can be utilized for better classification.
- There seems to be little understanding of how such models can be deployed in clinical settings. Hence, in the future, explainable artificial intelligence (XAI) can be used to understand working of model by highlighting the abnormal regions by using Shapley, LIME or Grad-CAM EAI tools.

6. Challenges in deep learning

A notable challenge is the requirement for vast amounts of training data to construct good DL models. Transfer learning can overcome this limitation using training data from related tasks [97]. However, the transferred data do not completely supplant the need for original data. Nevertheless, they improve the initial input data representation and its mapping function, thereby enhancing the model's performance [98]. Another challenge is unbalanced data, a frequent occurrence with biological data, where negative samples typically outnumber positive samples. When using skewed data to train a DL model, unexpected results might occur. The impact of imbalanced data on the DL model's performance has been well studied [99]. Another challenge is uncertainty scaling. In healthcare and related applications, uncertainty scaling is often used to assess the accuracy of automated ML and DL-based diagnoses [100]. Overconfident predictions can occur in DL models, with the probability score derived from the direct SoftMax output being frequently off the mark [101]. Another issue with DL is catastrophic forgetting [102], which occurs when new information incorporated into simple DL models interferes with previously learned information [103]. A solution to this problem involves training a new model from scratch using old and new data [102]. DL models risk data overfitting during the training stage due to the many parameters involved, many of which are interrelated [104,105]. This impairs the model's ability to perform effectively [106]. Inadequate training data can lead to overfitting, which causes the learned distribution to deviate from the true distribution [107]. The vanishing gradient problem emerges when employing backpropagation and gradient-based

learning approaches with artificial neural networks, especially during training [108–110]. Every weight of the neural network is updated depending on the current weight and is proportionately relevant to the partial derivative of the error function during each training iteration [111–114]. However, this weight update may not occur in some situations due to a vanishing gradient or progressively decreasing to tiny. As a result, no more training is feasible, and the neural network will be terminated [115,116].

DL is highly data-intensive. The many DL techniques for measuring human health status and the variety of available subject-specific data have become significantly more sophisticated and greater in size, necessitating higher computing power. To solve the mathematical equations associated with DL, parallel processing technologies like graphics processing units and field-programmable gate arrays are increasingly being used [117]. Alternatively, model compression [118] may be deployed to reduce the computational demands of DL models, so they may be feasibly deployed on machines with low processing capability, particularly in remote geographies where healthcare resources are limited [119].

7. Future aspects

DL models can be developed that not only detect SZ, but also may be used to monitor disease progression and optimize therapy, e.g., through selection and iteration of pharmacological treatments. For the training of DL networks, simpler models with fewer layers and less computational demands should be constructed and favoured over-complicated models. Further, deploying designs combining attention networks with external memory modules capable of mapping connections between individuals is an attractive avenue for future research.

The availability of accessible training SZ datasets for research is a fundamental hurdle that limits the development of DL models. Enrolling more subjects in these datasets should be encouraged to address this issue. In addition, using standardized terms and reporting metrics would facilitate a more precise evaluation of the model's reliability, robustness, and generalizability. Finally, researchers should have access to relevant sex- and age-specific group data to develop clinically meaningful DL models for diverse at-risk populations. In our review, the studies have largely focused on the binary classification of SZ vs. HC. Future research can focus on distinguishing the various forms of SZ [120], which may refine the diagnosis and assist with treatment choices.

Creating an ecosystem that connects the DL model via the cloud to the hospital and patient will facilitate remote DL-assisted expert diagnosis and provision of continued care. While EEG signals are now more commonly employed as adjunctive clinical diagnostic aid for SZ detection, we envision that, with more research efforts, clinical neuroimaging modalities like sMRI, pMRI, dMRI and PET can be efficiently incorporated into this future DL-enabled SZ diagnostic and management healthcare ecosystem.

8. Conclusion

SZ is a mental condition that impairs higher brain function with devastating consequences. EEG and neuroimaging provide information on brain structure and/or function that may be exploited for diagnostic screening. However, these signals generate high-volume data that are onerous to interpret manually. DL offers a one-stop classification of input signals without needing handcrafted feature engineering. In this review, we surveyed contemporary DL and composite models for SZ detection. Discussion of the techniques employed, their advantages and disadvantages, and the challenges of DL methods will provide researchers with a valuable resource to develop novel DL models that will improve SZ diagnosis and its management.

References

[1] Ahmad Shalbaf· Sara Bagherzadeh2· Arash Maghsoudi,Transfer learning with deep convolutional neural network for automated detection of schizophrenia from EEG signals https://link.springer.com/article/10.1007/s13246-020-00925-9.
[2] National Institute of Mental Health. Schizophrenia; National Institute of Mental Health: Bethesda, MD, USA, 2016.

[3] Kay, S.R.; Fiszbein, A.; Opler, L.A. The positive and negative syndrome scale (PANSS) for schizophrenia. Schizophr. Bull. 1987, 13, 261–276.
[4] 26. Lai, J.W.; Ang, C.K.E.; Acharya, U.R.; Cheong, K.H. Schizophrenia: A Survey of Artificial Intelligence Techniques Applied to Detection and Classification. Int. J. Environ. Res. Public Health 2021, 18, 6099. https://doi.org/10.3390/ ijerph18116099.
[5] Appaji ,Vaishak Harish ,Vittal Korann ,Priyanka Devi , Arpitha Jacob , Anantha Padmanabha , Vijay Kumar , Shiv-arama Varambally ,Ganesan Venkatasubramanian , Shyam Vasudeva Rao ,H.N. Suma , Caroll A.B. Webers , Tos T.J.M. Berendschot , Naren P. Rao„"Deep learning model using retinal vascular images forclassifying schizophrenia Abhishek" https://www.sciencedirect.com/science/article/abs/pii/S0920996422000688?via%3Dihub.
[6] Aslan Z, Akın M (2020) Automatic detection of schizophrenia by applying deep learning over spectrogram images of EEG signals.
[7] 5. David Ahmedt-Aristizabal, Tharindu Fernando, Simon Denman, Jonathan E. Robinson, Sridha Sridharan Patrick J. John-ston, Kristin R. Laurens, Clinton Fookes,"Identification of Children At Risk of Schizophrenia via Deep Learning and EEG Responses",https://pubmed.ncbi.nlm.nih.gov/32310808/
[8] Kuldeep Singh , Sukhjeet Singh and Jyoteesh Malhotra, Spectral features based convolutional neural network for accurate and prompt identification of schizophrenic patients https://pubmed.ncbi.nlm.nih.gov/33124526/: :text=The%20overall%20analysis %20of%20simulation,and%2098.56%25%20for%20two%20different.
[9] J. Satheesh Kumar; P. Bhuvaneswari (2012). Analysis of Electroencephalography (EEG) Signals and Its Categorization–A Study. doi:10.1016/j.proeng.2012.06.298.
[10] Brandon Westover M, David M. Greer, Emily Choi and Karim M. Awad. Pocket Neurology: Spiral Bound; 2010.
[11] Thoru Yamada and Elizabeth Meng Practical Guide for Clinical Neurophysiologic Testing: EEG: NIH Publication
[12] Jasper HH. The ten-twenty electrode system of the International Federation. Electroencephalography and clinical neurophysiology.1958; 10: 371-5.
[13] https://openfmri.org/dataset/ds000030/
[14] Pinkham, A.; Loughead, J.; Ruparel, K.; Wu, W.C.; Overton, E.; Gur, R.; Gur, R. Resting quantitative cerebral blood flow in schizophrenia measured by pulsed arterial spin labeling perfusion MRI. Psychiatry Res. Neuroimaging 2011, 194, 64–72.
[15] Korfiatis, P.; Erickson, B. The basics of diffusion and perfusion imaging in brain tumors. Appl. Radiol. 2014, 43, 22.
[16] Kubicki, M.; McCarley, R.; Westin, C.F.; Park, H.J.; Maier, S.; Kikinis, R.; Jolesz, F.A.; Shenton, M.E. A review of diffusion tensor imaging studies in schizophrenia. J. Psychiatr. Res. 2007, 41, 15–30.
[17] Kyriakopoulos, M.; Bargiotas, T.; Barker, G.J.; Frangou, S. Diffusion tensor imaging in schizophrenia. Eur. Psychiatry 2008, 23, 255–273.
[18] Qureshi, Muhammad Naveed Iqbal; Oh, Jooyoung; Lee, Boreom (2019). 3D-CNN based discrimination of schizophrenia using resting-state fMRI. Artificial Intelligence in Medicine, 98(), 10–17. doi:10.1016/j.artmed.2019.06.003.
[19] Zhang Z, Cui P, Zhu W. Deep learning on graphs: a survey. IEEE Trans Knowl Data Eng. 2020. https:// doi. org/ 10. 1109/ TKDE. 2020. 29813 33.
[20] Shrestha A, Mahmood A. Review of deep learning algorithms and architectures. IEEE Access. 2019;7:53040–65.
[21] Najafabadi MM, Villanustre F, Khoshgoftaar TM, Seliya N, Wald R, Muharemagic E. Deep learning applications and challenges in big data analytics. J Big Data. 2015;2(1):1.
[22] Goodfellow I, Bengio Y, Courville A, Bengio Y. Deep learning, vol. 1. Cambridge: MIT press; 2016.
[23] Shorten C, Khoshgoftaar TM, Furht B. Deep learning applications for COVID-19. J Big Data. 2021;8(1):1–54.
[24] Krizhevsky A, Sutskever I, Hinton GE. Imagenet classification with deep convolutional neural networks. Commun ACM. 2017;60(6):84–90.
[25] He K, Zhang X, Ren S, Sun J. Deep residual learning for image recognition. In: Proceedings of the IEEE conference on computer vision and pattern recognition; 2016. p. 770–8.
[26] https://www.ibm.com/cloud/learn/deep-learning
[27] Van Essen B, Kim H, Pearce R, Boakye K, Chen B. Lbann: livermore big artificial neural network HPC toolkit. In: Proceedings of the workshop on machine learning in high-performance computing environments; 2015. p. 1–6.
[28] Laith Alzubaidi;Jinglan Zhang;Amjad J. Humaidi;Ayad Al-Dujaili;Ye Duan;Omran Al-Shamma;J. Santamaría;Mohammed A. Fadhel;Muthana Al-Amidie;Laith Farhan; (2021). Review of deep learning: concepts, CNN architectures, challenges, applications, future directions . Journal of Big Data, (), –. doi:10.1186/s40537-021-00444-8
[29] Luxton, D.D. Artificial Intelligence in Behavioral and Mental Health Care; Academic Press: Cambridge, MA, USA, 2015.
[30] Hamet, P.; Tremblay, J. Artificial intelligence in medicine. Metabolism 2017, 69, S36–S40.
[31] Liang, Y.; Zheng, X.; Zeng, D.D. A survey on big data-driven digital phenotyping of mental health. Inf. Fusion 2019, 52, 290–307
[32] S. M. Plis, et al., “Deep learning for neuroimaging: A validation study,” Front. Neurosci., vol. 8, pp. 229, 2014.
[33] S. L. Oh, J. Vicnesh, E. J. Ciaccio, R. Yuvaraj, and U. R. Acharya, “Deep convolutional neural network model for auto-mated diagnosis of schizophrenia using EEG signals,” Appl. Sci., vol. 9, no. 14, p. 2870, 2019. [Online]. Available: https://www.mdpi.com/2076-3417/9/14/2870
[34] Olejarczyk, E.; Jernajczyk, W. Graph-based analysis of brain connectivity in schizophrenia. PLoS ONE 2017, 12, e0188629. https://journals.plos.org/plosone/article?id=10.1371/journal.pone.0188629.
[35] 2.Smith K. Khare; Varun Bajaj; U. Rajendra Acharya, SPWVD-CNN for Automated Detection of Schizophrenia Patients Using EEG Signals, doi:10.1109/TIM.2021.3070608.
[36] J. M. Ford, V. A. Palzes, B. J. Roach, and D. H. Mathalon, “Did I do that? Abnormal predictive processes in schizophrenia when button pressing to deliver a tone,” Schizophrenia Bull., vol. 40, no. 4, pp. 804–812, Jul. 2014.
[37] Kaggle: Your Machine Learning and Data Science Community. Accessed: Feb. 22, 2020. [Online]. Available: https://www.kaggle.com/broach/button-tone-sz.
[38] Phang, Chun-Ren; Ting, Chee-Ming; Noman, Fuad; Ombao, Hernando.Classification of EEG-Based Brain Connectivity Networks in Schizophrenia Using a Multi-Domain Connectome Convolutional Neural Network.https://arxiv.org/abs/1903.08858
[39] N. N. Gorbachevskaya and S. Borisov, “EEG data of healthy adolescents and adolescents with symptoms of schizophrenia,"".
[40] Shrinidhi Sridhar, et. al, " Deep Learning-Based Diagnosis Of Schizophrenia ", https://turcomat.org/index.php/turkbilmat/article/view/7997
[41] Lorenzo Santos Mayo, Luis M. San José Revuelta and Juan Ignacio Arribas, A computer aided diagnosis system with EEG based on the P3b wave during an auditory odd ball task in schizophrenia, Trait du Signal.https://doi.org/10.18280/ts.370209
[42] Borisov SV, Kaplan AY, Gorbachevskaya NL, Kozlova IA (2005) Analysis of EEG structural synchrony in adolescents with schizophrenic disorders. Hum Physiol.
[43] Nikhil Chandran, Karthik Sreekumar, and D. P. Subha, "EEG-Based Automated Detection of Schizophrenia Using Long Short-Term Memory (LSTM) Network","https://doi.org/10.1007/978-981-15-5243-4_19".
[44] http://cobre.mrn.org/
[45] Yang, Bo, et al. "Schizophrenia classification using fMRI data based on a multiple feature image capsule network ensemble." IEEE Access 7 (2019): 109956-109968.
[46] https://openfmri.org/.VOLUME 7, 2019
[47] Campese, Stefano, et al. "Psychiatric disorders classification with 3D convolutional neural networks." INNS Big Data and Deep Learning Conference. Springer, Cham, 2019.
[48] Niu, Yan-Wei, et al. "Sample augmentation for classification of schizophrenia patients and healthy controls using ICA of fMRI data and convolutional neural networks." 2019 Tenth International Conference on Intelligent Control and Information Processing (ICICIP). IEEE, 2019.
[49] Kuang, Li-Dan; Lin, Qiu-Hua; Gong, Xiao-Feng; Cong, Fengyu; Sui, Jing; Calhoun, Vince D. (2018). Model Order Effects on ICA of Resting-State Complex-Valued fMRI Data: Application to Schizophrenia. Journal of Neuroscience Methods, (), S0165027018300438–. doi:10.1016/j.jneumeth.2018.02.013
[50] Yan, Weizheng, et al. "Discriminating schizophrenia using recurrent neural network applied on time courses of multi-site FMRI data." EBioMedicine 47 (2019): 543-552.

[51] Qiu, Yue, et al. "Classification of schizophrenia patients and healthy controls using ICA of complex-valued fMRI data and convolutional neural networks." International Symposium on Neural Networks. Springer, Cham, 2019.
[52] Oh, Kanghan, et al. "Classification of schizophrenia and normal controls using 3D convolutional neural network and outcome visualization." Schizophrenia research 212 (2019): 186-195.
[53] Noor, Manan Binth Taj, et al. "Detecting neurodegenerative disease from MRI: a brief review on a deep learning perspective." International conference on brain informatics. Springer, Cham, 2019.
[54] Pinaya, Walter HL, et al. "Using deep belief network modelling to characterize differences in brain morphometry in schizophrenia." Scientific reports 6.1 (2016): 1-9.
[55] Patel, Pinkal, Priya Aggarwal, and Anubha Gupta. "Classification of schizophrenia versus normal subjects using deep learning." Proceedings of the Tenth Indian Conference on Computer Vision, Graphics and Image Processing. 2016.
[56] Yan, Weizheng, et al. "Discriminating schizophrenia from normal controls using resting state functional network connectivity: A deep neural network and layer-wise relevance propagation method." 2017 IEEE 27th international workshop on machine learning for signal processing (MLSP). IEEE, 2017.
[57] Han, Shaoqiang, et al. "Recognition of early-onset schizophrenia using deep-learning method." Applied Informatics. Vol. 4. No. 1. SpringerOpen, 2017.
[58] Dakka, Jumana, et al. "Learning neural markers of schizophrenia disorder using recurrent neural networks." arXiv preprint arXiv:1712.00512 (2017).
[59] Latha, Manohar, and Ganesan Kavitha. "Detection of Schizophrenia in brain MR images based on segmented ventricle region and deep belief networks." Neural Computing and Applications 31.9 (2019): 5195-5206.
[60] Zeng, Ling-Li, et al. "Multi-site diagnostic classification of schizophrenia using discriminant deep learning with functional connectivity MRI." EBioMedicine 30 (2018): 74-85.
[61] Matsubara, Takashi, Tetsuo Tashiro, and Kuniaki Uehara. "Deep neural generative model of functional MRI images for psychiatric disorder diagnosis." IEEE Transactions on Biomedical Engineering 66.10 (2019): 2768-2779.
[62] Srinivasagopalan, Srivathsan, et al. "A deep learning approach for diagnosing schizophrenic patients." Journal of Experimental Theoretical Artificial Intelligence 31.6 (2019): 803-816.
[63] Lin, Qiu-Hua, et al. "SSPNet: An interpretable 3D-CNN for classification of schizophrenia using phase maps of resting-state complex-valued fMRI data." Medical Image Analysis 79 (2022): 102430.
[64] https://www.nimh.nih.gov/health/statistics/schizophrenia
[65] Lei Chu, Robert Qiu, Haichun Liu, Zenan Ling, Tianhong Zhang and Jijun Wang,Individual Recognition in Schizophrenia using Deep Learning Methods with Random Forest and Voting Classifiers: Insights from Resting State EEG Streams, https://arxiv.org/abs/1707.03467
[66] Maryam Saeedi ,Abdolkarim Saeedi, Pooya Mohammadi,"Schizophrenia Diagnosis via FFT and Wavelet Convolutional Neural Networks utilizing EEG signals", "https://assets.researchsquare.com/files/rs-1497490/v1_covered.pdf?c=1648654087".
[67] Afshin Shoeibi , Delaram Sadeghi , Parisa Moridian, Navid Ghassemi , Jónathan Heras , Roohallah Alizadehsani , Ali Khadem, Yinan Kong, Saeid Nahavandi , Yu-Dong Zhang and Juan Manuel Gorriz ,Automatic Diagnosis of Schizophrenia in EEG Signals Using CNN-LSTM Models https://www.frontiersin.org/articles/10.3389/fninf.2021.777977/full.
[68] Jie Sun1, Rui Cao2, Mengni Zhou3, Waqar Hussain1, Bin Wang1, Jiayue Xue1 Jie Xiang,A hybrid deep neural network for classification of schizophrenia using EEG Data https://www.nature.com/articles/s41598-021-83350-6.
[69] Phang, Chun-Ren, et al. "Classification of EEG-based brain connectivity networks in schizophrenia using a multi-domain connectome convolutional neural network." arXiv preprint arXiv:1903.08858 (2019).
[70] Abinaya Sundari R, C M Sujatha, Identification of Schizophrenia using LSTM Recurrent Neural Network https://ieeexplore.ieee.org/document/9445189
[71] Faust, O.; Hagiwara, Y.; Hong, T.J.; Lih, O.S.; Acharya, U.R. Deep learning for healthcare applications based on physiological signals: A review. Comput. Methods Programs Biomed. 2018, 161, 1–13.
[72] Lecun, Y.; Bengio, Y.; Hinton, G. Deep learning. Nature 2015, 521, 436–444.
[73] Scherer, D.; Müller, A.; Behnke, S. Evaluation of pooling operations in convolutional architectures for object recognition. Lect. Notes Comput. Sci. 2010, 6354 LNCS Pt 3, 92–101.
[74] Serre, T.; Wolf, L.; Poggio, T. Object recognition with features inspired by visual cortex. In Proceedings of the 2005 IEEE Computer Society Conference on Computer Vision and Pattern Recognition; CVPR 2005, San Diego, CA, USA, USA, 20–25 June 2005; pp. 994–1000.
[75] https://www.upgrad.com/blog/basic-cnn-architecture/
[76] Aslan Z (2019) On the use of deep learning methods on medical images. Int J Energy Eng Sci 3(2):1–15
[77] Eren, Levent; Ince, Turker; Kiranyaz, Serkan (2018). A Generic Intelligent Bearing Fault Diagnosis System Using Compact Adaptive 1D CNN Classifier. Journal of Signal Processing Systems, (), –. doi:10.1007/s11265-018-1378-3
[78] Starke, S., Leger, S., Zwanenburg, A., Leger, K., Lohaus, F., Linge, A., . . . Löck, S. (2020). 2D and 3D convolutional neural networks for outcome modelling of locally advanced head and neck squamous cell carcinoma. Scientific Reports, 10(1). doi:10.1038/s41598-020-70542-9
[79] Rao, C., Liu, Y. (2020). Three-dimensional convolutional neural network (3D-CNN) for heterogeneous material homogenization. Computational Materials Science, 184, 109850. doi:10.1016/j.commatsci.2020.1098
[80] Y. LeCun, B. Boser, J.S. Denker, D. Henderson, R.E. Howard, W. Hubbard, L.D. Jackel, Backpropagation applied to handwritten zip code recognition, Neural Comput. 1 (4) (1989) 541–551.
[81] C.M. Bishop, et al., Neural networks for pattern recognition, Oxford University Press, 1995.
[82] F. Girosi, M. Jones, T. Poggio, Regularization theory and neural networks architectures, Neural Comput. 7 (2) (1995) 219–269.
[83] Sepp Hochreiter; Jürgen Schmidhuber (1997). "Long short-term memory". Neural Computation. 9 (8): 1735–1780. doi:10.1162/neco.1997.9.8.1735. PMID 9377276. S2CID 1915014
[84] Graves, A.; Liwicki, M.; Fernández, S.; Bertolami, R.; Bunke, H.; Schmidhuber, J. (May 2009). "A Novel Connectionist System for Unconstrained Handwriting Recognition". IEEE Transactions on Pattern Analysis and Machine Intelligence. 31 (5): 855–868. CiteSeerX 10.1.1.139.4502. doi:10.1109/tpami.2008.137. ISSN 0162-8828. PMID 19299860. S2CID 14635907
[85] Li, Xiangang; Wu, Xihong (2014-10-15). "Constructing Long Short-Term Memory based Deep Recurrent Neural Networks for Large Vocabulary Speech Recognition". arXiv:1410.4281
[86] Mayer, H.; Gomez, F.; Wierstra, D.; Nagy, I.; Knoll, A.; Schmidhuber, J. (October 2006). A System for Robotic Heart Surgery that Learns to Tie Knots Using Recurrent Neural Networks. 2006 IEEE/RSJ International Conference on Intelligent Robots and Systems. pp. 543–548. CiteSeerX 10.1.1.218.3399. doi:10.1109/IROS.2006.282190. ISBN 978-1-4244-0258-8. S2CID 12284900
[87] Hochreiter, Sepp; Schmidhuber, Juergen (1996). LSTM can solve hard long time lag problems. Advances in Neural Information Processing Systems
[88] Felix A. Gers; Jürgen Schmidhuber; Fred Cummins (2000). "Learning to Forget: Continual Prediction with LSTM". Neural Computation. 12 (10): 2451–2471. CiteSeerX 10.1.1.55.5709. doi:10.1162/089976600300015015. PMID 11032042. S2CID 11598600
[89] https://viso.ai/deep-learning/resnet-residual-neural-network/
[90] https://iq.opengenus.org/resnet50-architecture/: :text=ResNet50%20is%20a%20variant%20of,explored%20ResNet50%20architecture%20in%20depth.
[91] 56. https://towardsdatascience.com/step-by-step-vgg16-implementation-in-keras-for-beginners-a833c686ae6c: :text=VGG16%20is%20a%20convolution %20neural,vision%20model%20architecture%20till%20date.
[92] Bose, Thilakavathi; Sivakumar, Shenbaga Devi; Kesavamurthy, Bhanu . Identification of Schizophrenia Using EEG Alpha Band Power During Hyperventilation and Post-hyperventilation. Journal of Medical and Biological Engineering,2016, 36(6) 901–911. doi:10.1007/s40846-016-0192.
[93] Yan, Weizheng; Calhoun, Vince; Song, Ming; Cui, Yue; Yan, Hao; Liu, Shengfeng; Fan, Lingzhong; Zuo, Nianming; Yang, Zhengyi; Xu, Kaibin; Yan, Jun; Lv, Luxian; Chen, Jun; Chen, Yunchun; Guo, Hua; Li, Peng; Lu, Lin; Wan, Ping; Wang, Huaning; Wang, Huiling; Yang, Yongfeng; Zhang, Hongxing; Zhang, Dai; Jiang, Tianzi; Sui, Jing . Discriminating schizophrenia using recurrent neural networks applied on time courses of multi-site FMRI data. EBioMedicine,2019 (), S2352396419305456–. doi:10.1016/j.ebiom.2019.08.023.

[94] Ingalhalikar, M.; Kanterakis, S.; Gur, R.; Roberts, T.P.; Verma, R. DTI based diagnostic prediction of a disease via pattern classification. In Proceedings of the International Conference on Medical Image Computing and Computer-Assisted Intervention, Beijing, China, 20–24 September 2010; Springer: Berlin/Heidelberg, Germany, 2010; pp. 558–565.
[95] Caprihan, A.; Pearlson, G.D.; Calhoun, V.D. Application of principal component analysis to distinguish patients with schizophrenia from healthy controls based on fractional anisotropy measurements. Neuroimage 2008, 42, 675–682.
[96] 148. J. M. Bruggemann, H. V. Stockill, R. K. Lenroot, and K. R. Laurens, "Mismatch negativity (MMN) and sensory auditory processing in children aged 9–12 years presenting with putative antecedents of schizophrenia," International journal of psychophysiology, vol. 89, no. 3, pp. 374–380, 2013.
[97] Tan C, Sun F, Kong T, Zhang W, Yang C, Liu C. A survey on deep transfer learning. In: International conference on artificial neural networks. Springer; 2018. p. 270–9.
[98] Weiss K, Khoshgoftaar TM, Wang D. A survey of transfer learning. J Big Data. 2016;3(1):9.
[99] Pan W. A survey of transfer learning for collaborative recommendation with auxiliary data. Neurocomputing. 2016;177:447–53.
[100] Johnson JM, Khoshgoftaar TM. Survey on deep learning with class imbalance. J Big Data. 2019;6(1):27.
[101] Yang P, Zhang Z, Zhou BB, Zomaya AY. Sample subset optimization for classifying imbalanced biological data. In: Pacific-Asia conference on knowledge discovery and data mining. Springer; 2011. p. 333–44.
[102] Yang P, Yoo PD, Fernando J, Zhou BB, Zhang Z, Zomaya AY. Sample subset optimization techniques for imbalanced and ensemble learning problems in bioinformatics applications. IEEE Trans Cybern. 2013;44(3):445–55.
[103] Li Y, Huang C, Ding L, Li Z, Pan Y, Gao X. Deep learning in bioinformatics: introduction, application, and perspective in the big data era. Methods. 2019;166:4–21.
[104] Nair T, Precup D, Arnold DL, Arbel T. Exploring uncertainty measures in deep networks for multiple sclerosis lesion detection and segmentation. Med Image Anal. 2020;59:101557.
[105] Herzog L, Murina E, Dürr O, Wegener S, Sick B. Integrating uncertainty in deep neural networks for MRI based stroke analysis. Med Image Anal. 2020;65:101790.
[106] Lee K, Lee K, Shin J, Lee H. Overcoming catastrophic forgetting with unlabeled data in the wild. In: Proceedings of the IEEE international conference on computer vision; 2019. p. 312–21.
[107] Shmelkov K, Schmid C, Alahari K. Incremental learning of object detectors without catastrophic forgetting. In: Proceedings of the IEEE international conference on computer vision; 2017. p. 3400–09.
[108] Cheng Y, Wang D, Zhou P, Zhang T. Model compression and acceleration for deep neural networks: the principles, progress, and challenges. IEEE Signal Process Mag. 2018;35(1):126–36.
[109] Wiedemann S, Kirchhoffer H, Matlage S, Haase P, Marban A, Marin˜c T, Neumann D, Nguyen T, Schwarz H, Wiegand T, et al. Deepcabac: a universal compression algorithm for deep neural networks. IEEE J Sel Topics Signal Process. 2020;14(4):700–14.
[110] Mehta N, Pandit A. Concurrence of big data analytics and healthcare: a systematic review. Int J Med Inform. 2018;114:57–65.
[111] Xu Q, Zhang M, Gu Z, Pan G. Overfitting remedy by sparsifying regularization on fully-connected layers of CNNs. Neurocom- puting. 2019;328:69–74.
[112] Zhang C, Bengio S, Hardt M, Recht B, Vinyals O. Understanding deep learning requires rethinking generalization. Commun ACM. 2018;64(3):107–15.
[113] Xu X, Jiang X, Ma C, Du P, Li X, Lv S, Yu L, Ni Q, Chen Y, Su J, et al. A deep learning system to screen novel coronavirus disease 2019 pneumonia. Engineering. 2020;6(10):1122–9.
[114] Wang X, Qin Y, Wang Y, Xiang S, Chen H. ReLTanh: an activation function with vanishing gradient resistance for SAE-based DNNs and its application to rotating machinery fault diagnosis. Neurocomputing. 2019;363:88–98.
[115] Tan HH, Lim KH. Vanishing gradient mitigation with deep learning neural network optimization. In: 2019 7th international conference on smart computing communications (ICSCC). IEEE; 2019. p. 1–4.
[116] MacDonald G, Godbout A, Gillcash B, Cairns S. Volume-preserving neural networks: a solution to the vanishing gradient problem; 2019. arXiv preprint arXiv:1911.09576.
[117] Platt J, et al. Probabilistic outputs for support vector machines and comparisons to regularized likelihood methods. Adv Large Margin Classif. 1999;10(3):61–74.
[118] Choi E, Bahadori MT, Sun J, Kulas J, Schuetz A, Stewart W. Retain: An interpretable predictive model for healthcare using reverse time attention mechanism. In: Advances in neural information processing systems. San Mateo: Morgan Kaufmann Publishers; 2016. p. 3504–12.
[119] Ching T, Himmelstein DS, Beaulieu-Jones BK, Kalinin AA, Do BT, Way GP, Ferrero E, Agapow PM, Zietz M, Hoffman MM, et al. Opportunities and obstacles for deep learning in biology and medicine. J R Soc Interface. 2018;15(141):20170,387.
[120] Harper, A. E., Jr. (1950). Discrimination of the types of schizophrenia by the Wechsler-Bellevue scale. Journal of Consulting Psychology, 14(4), 290–296. https://doi.org/10.1037/h0060181
[121] Alom, M.Z., Taha, T.M., Yakopcic, C., Westberg, S., Sidike, P., Nasrin, M.S., Van Esesn, B.C., Awwal, A.A.S. and Asari, V.K., 2018. The history began from alexnet: A comprehensive survey on deep learning approaches. *arXiv preprint arXiv:1803.01164*.
[122] https://www.simplilearn.com/tutorials/deep-learning-tutorial/deep-learning-algorithm
[123] Bhatt, Umang, et al. "Explainable machine learning in deployment." *Proceedings of the 2020 conference on fairness, accountability, and transparency*. 2020.
[124] Loh, Hui Wen, et al. "Application of Explainable Artificial Intelligence for Healthcare: A Systematic Review of the Last Decade (2011–2022)." *Computer Methods and Programs in Biomedicine* (2022): 107161.
[125] Sharma, M., Acharya, U.R. Automated detection of schizophrenia using optimal wavelet-based l1l1 norm features extracted from single-channel EEG. Cogn Neurodyn 15, 661–674 (2021). https://doi.org/10.1007/s11571-020-09655-w